Time-reversal duality of high-efficiency RF power amplifiers

T. Reveyrand, I. Ramos and Z. Popović

Published in
Electronics Letters, 6th December 2012 Vol. 48 No. 25, pp.1607-1608.

Crossref DOI: 10.1049/el.2012.3004

Time-reversal duality of high-efficiency RF power amplifiers

T. Reveyrand, I. Ramos and Z. Popović

The similarity between RF power amplifiers and rectifiers is discussed. It is shown that the same high-efficiency harmonically-terminated power amplifier can be operated in a dual rectifier mode. Nonlinear simulations with a GaN HEMT transistor model show the time-reversal intrinsic voltage and current waveform relationship between a class-F amplifier and rectifier. Measurements on a class-F^{-1} amplifier and rectifier at 2.14 GHz demonstrate over 80% efficiency in both cases.

Introduction: High-efficiency RF power amplifiers (PAs) are designed by presenting appropriate output impedances at the fundamental and harmonic frequencies, shaping the current and voltage waveforms across the current source of the device to minimise the power dissipation $v(t) \times i(t)$. In the past few years, PAs implemented in GaN technology have demonstrated power added efficiencies (PAEs) above 80% using a single transistor. In this Letter, we show that a harmonically-terminated transistor amplifier is a bidirectional device that exibits high efficiency in both amplifier and rectifier modes. High power conversion efficiency of a power amplifier (DC to RF) and a rectifier obtained by operating the amplifier in reverse (RF to DC) is achieved with time-reversal duality [1] of the transistor's main current source. In other words, the power amplifier (PA) and rectifier (R) drain terminal voltage and current are related by $v_{PA}(t) = v_R(t)$ and $i_{PA}(t) = -i_R(t)$. The block diagram in Fig. 1 shows the main PA and rectifier parameters that are discussed here. The matching networks are designed to optimise PA efficiency for a 50 Ω load and are not changed for rectifier mode operation.

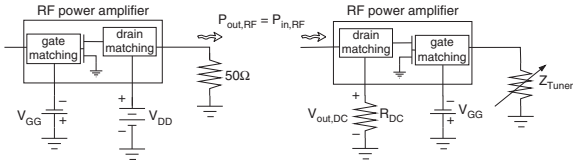

Fig. 1 *Block diagram of power amplifier circuit operated in PA mode (left) and rectifier mode (right)*

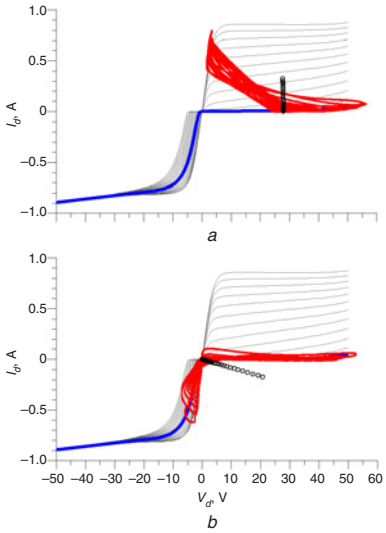

Fig. 2 *Simulated GaN transistor I-V curves (grey), dynamic load lines (red) and drain DC voltage and current (black) for PA of Fig. 2a and rectifier (Fig. 2b). Blue line is $V_{gs} = -4.9V$ transistor characteristic (gate bias point value for both cases). Time-reversal duality is seen as RF power at drain and is swept from 0 to 40 dBm at 2.14 GHz. PA case has drain bias of 28 V*

In the remainder of the Letter, example simulations of a class-F amplifier based on a GaN HEMT illustrate the time-reversal duality of power amplifiers and rectifiers. Nonlinear simulations result in time-reversed dual current and voltage waveforms at the virtual drain of the PA and rectifier. After the principle is demonstrated though simulations of intrinsic waveforms, measurements on a class-F^{-1} GaN power amplifier using a TriQuint device are compared for PA and rectifier configurations, with the goal of demonstrating that this duality holds for various high-efficiency amplifier and rectifier circuits.

Simulations of PA and rectifier: Simulations have been performed with the 8 × 75 μm GaN HEMT model described in [2] at 2.14 GHz. This nonlinear model includes: nonlinear capacitances C_{gs}, C_{gd} and C_{ds}; gate-souce and gate-drain diodes; and breakdown and trapping effects. This model reproduces the nonlinear transistor behaviour not only for positive but also for negative values of the drain voltage.

For the amplifier mode of operation, when an input RF signal is injected into the gate terminal, we consider the drain efficiency, or DC-to-RF conversion efficiency: $\eta_{PA} = P_{out,RF}/P_{DC}$ In class-F mode with five harmonics terminated, for $V_{ds} = 28V$ and $V_{gs} = -4.9V$, an amplifier efficiency $\eta_{PA} = 72\%$ is obtained. The simulated behaviour of the transistor is depicted on Figs. 2*a* and 3*a*, showing the *I-V* curves and load-line, and intrinsic drain voltage and current waveforms, respectively.

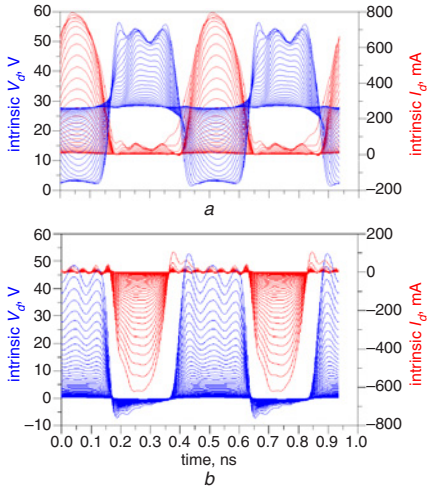

Fig. 3 *Simulated time-domain intrinsic drain voltage (blue) and current (red) waveforms for varying RF power at drain for PA (Fig. 3a) and rectifier (Fig. 3b). In the case of PA, $V_{ds} = 28V$*

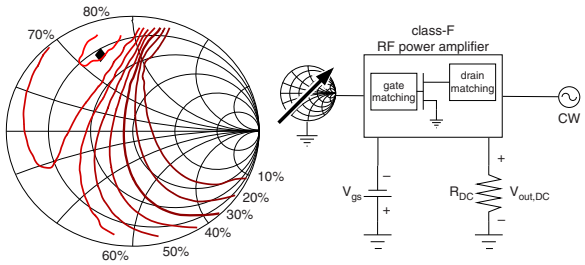

Fig. 4 *Load-pull simulations for rectifier efficiency obtained at transistor terminals. Frequency is 2.45 GHz and RF drain input power is 40 dBm. Diamond symbol shows impedance for maximal efficiency*

The same class-F PA circuit is next simulated in rectifier mode, where the drain DC power supply is replaced by a DC load R_{DC}. The input to the circuit is now RF power $P_{in,RF}$ equal to $P_{out,RF}$ of the amplifier, and injected at the drain port as illustrated in Fig. 4. Assuming the DC gate current is negligible, the rectifier RF-to-DC conversion efficiency is

$$\eta_R = \frac{P_{DC}}{P_{in,RF}} = \frac{2|V_{DC}|^2}{R_{DC}\Re\{V_{drain}(f_0)I^*_{drain}(f_0)\}} \quad (1)$$

An impedance tuner connected at the gate input of the PA allows load-pull at the gate resulting in $\eta_R = 80\%$ with $R_{DC} = 120\Omega$ ($f_{RF} =$ 2.14GHz). Figs. 2*b* and 3*b* illustrate the behaviour of the transistor for RF gate load impedance that maximises rectifier efficiency. The waveforms at the intrinsic drain of the transistor correspond to time-reversed class-F waveforms. The gate-port load-pull contours are displayed in Fig. 4. The Figure also shows the optimal impedance for η_R at f_{RF} which is related to a dynamic load-line with a minimal enclosed area, and close to the *I-V* characteristic given at constant V_{gs}.

Measurements of PA and rectifier: Measurements were performed on a single-transistor GaN class-F^{-1} power amplifier detailed in [3]. This hybrid PA uses a TriQuint TGF2023-02 12-W bare die, and gives $P_{out,RF} = 7$ W with over 84.6% PAE at a drain voltage of 31 V and with a 19 dB gain at 2.14 GHz. The output matching circuit is designed by load-pull and has terminated second and third harmonics which are designed to give class-F^{-1} waveforms at the virtual drain reference plane. The gate is matched for large-signal gain at 2.14 GHz. This PA, biased at $V_{gs} = -4.4$V, was characterised in rectifier mode, with the reference plane set at the coaxial drain-port connector. A time-domain load-pull setup (Fig. 5) was used to obtain load-pull results at $R_{DC} = 98\Omega$, shown in Fig. 5. The best rectifier efficiency $\eta_R = 85\%$ is obtained for $Z_{load} = (229 + j.9)\Omega$ at $P_{in,RF} = 41$ dBm with $V_{DC} = 31$ V.

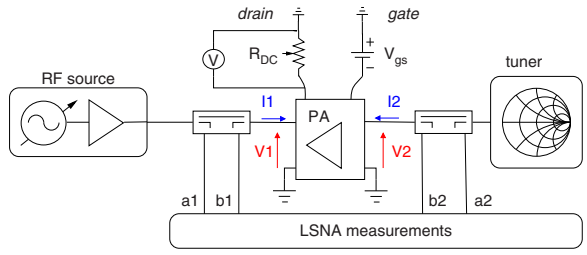

Fig. 5 *Rectifier load-pull measurement setup*
RF power sweep is performed at input drain port for each RF impedance provided by tuner at gate port

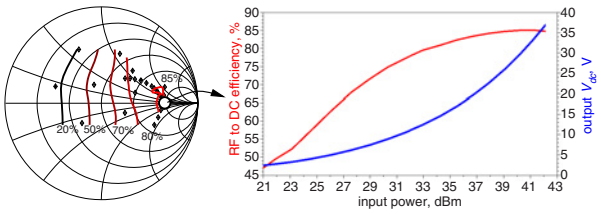

Fig. 6 *Rectifier performance measured at coaxial reference planes ($f_{RF} = 2.14$ GHz)*
Left: RF load impedances used for measurements (black dots), where contours correspond to max$\{\eta_R\}$ for the complete power sweep applied to RF drain port
Right: V_{DC} and η_R measured for $R_{DC} = 98\Omega$ and $Z_{load} = (229 + j.9)\Omega$

Discussion: While it was previously shown that harmonic terminations defined for power amplifier modes of operation can be used for diode and transistor rectifiers [4], the nonlinear simulations and experiments in this Letter demonstrate the time-reversal duality of high-efficiency microwave power amplifiers and rectifiers. In this case, the rectifier is obtained by operating the power amplifier in reverse mode, and the insight into transistor intrinsic waveforms is made possible by a GaN HEMT nonlinear model originally developped for switches. Over 80% conversion efficiency is demonstrated for both modes of circuit operation.

Note that the simulations and measurements for the rectifier are performed in self-synchronous mode, i.e. there is no input RF power incident externally into the gate port of the PA, unlike in previous lower-frequency transistor rectifier work [5, 6]. This is possible due to the non-negligible nonlinear feedback capacitance C_{gd}, which couples some of the input RF signal from the drain to the gate. In the class-F simulations, an isolation of 18 dB is observed between the drain and the gate ports with $C_{gd} \simeq 108$ fF. With the appropriate gate complex impedance the transistor can operate as a self-synchronous rectifier.

Acknowledgments: This work was funded in part by the Office of Naval Research under the DARPA MPC Program under grant N00014-11-1-0931, and in part by the Advanced Research Projects Agency-Energy (ARPA-E) Award DE-AR0000216.

25 August 2012
doi: 10.1049/el.2012.3004
One or more of the Figures in this Letter are available in colour online.

T. Reveyrand (*C2S2 Department, XLIM UMR 6172, 123 Avenue Albert Thomas, Limoges Cedex 87060, France*)

I. Ramos and Z. Popović (*Department of Electrical, Computer and Energy Engineering, University of Colorado, Boulder, CO 80309-0425, USA*)

E-mail: zoya.popovic@colorado.edu

References

1 Hamill, D.C.: 'Time reversal duality and the synthesis of a double class E DC-DC converter'. 21st Annual IEEE Power Electronics Specialists Conf., San Antonio, TX, USA, 1990, pp. 512–521
2 Callet, G., Faraj, J., Jardel, O., Charbonniaud, C., Jacquet, J.C., Reveyrand, T., Morvan, E., Piotrowicz, S., Teyssier, J.P., and Quéré, R.: 'A new nonlinear HEMT model for AlGaN/GaN switch applications', *Int. J. Microw. Wirel. Technol.*, 2010, **2**, (3–4), pp. 283–291
3 Roberg, M., Hoversten, J., and Popović, Z.: 'GaN HEMT PA with over 84% power added efficiency', *Electron. Lett.*, 2010, **46**, (23), pp. 1553–1554
4 Roberg, M., Falkenstein, E., and Popović, Z.: 'High-efficiency harmonically-terminated rectifier for wireless powering applications', IEEE MTT-S Int. Microwave Symp. Digest, Montreal, QC, Canada, 2012, pp. 1–3
5 Kazimierczuk, M.K., and Jozwik, J.J.: 'Analysis and design of class E zero-current-switching rectifier', *IEEE Trans. Circuits Syst.*, 1990, **37**, (8), pp. 1000–1009
6 Nieves Ruiz, M., Marante, R., and Garcia, J.A.: 'A class E synchronous rectifier based on an e-pHEMT device for wireless powering applications', IEEE MTT-S Int. Microwave Symp. Digest, Montreal, QC, Canada, 2012, pp. 252–255